

On the importance of intermolecular interactions of 3-(2,3-dihydroxy-isopentyl)-4-hydroxyacetophenone: Crystal structure, spectroscopic and hirshfeld surface analysis

Diego M. Gil ^{a,*,1}, Emilio Lizarraga ^{b,c}, Gustavo A. Echeverría ^d, Oscar E. Piro ^d, César A.N. Catalán ^e

^a INBIOFAL (CONICET – UNT), Instituto de Química Orgánica. Facultad de Bioquímica, Química y Farmacia. Universidad Nacional de Tucumán. Ayacucho 471, T4000INI, San Miguel de Tucumán. Argentina

^b Fundación Miguel Lillo, Instituto de Fisiología Animal, Miguel Lillo 251, T4000JFE, San Miguel de Tucumán, Argentina

^c Facultad de Ciencias Naturales e Instituto Miguel Lillo, Universidad Nacional de Tucumán, Miguel Lillo 205, T4000JFE, San Miguel de Tucumán, Argentina

^d Departamento de Física, Facultad de Ciencias Exactas, Universidad Nacional de La Plata and Institute IFLP (CONICET, CCT-La Plata), C. C. 67, 1900, La Plata, Argentina

^e Instituto de Química Orgánica. Facultad de Bioquímica, Química y Farmacia. Universidad Nacional de Tucumán, Ayacucho 471, T4000INI, San Miguel de Tucumán, Argentina

ARTICLE INFO

Article history:

Received 14 February 2020

Received in revised form

24 April 2020

Accepted 5 May 2020

Available online 10 May 2020

Keywords:

Hydrogen bonds

Non-covalent interactions

Hirshfeld surfaces

DFT

NBO analysis

ABSTRACT

The compound 3-(2,3-dihydroxy-isopentyl)-4-hydroxyacetophenone has been synthesized and characterized by ¹H Nuclear Magnetic Resonance (NMR), Infrared (IR) and Raman spectroscopies and its crystal structure was solved by single crystal X-ray diffraction. The molecular geometry of the compound was investigated theoretically by performing density functional theory (DFT) calculations to access reliable results to the experimental data. The substance crystallizes in the triclinic *P* $\bar{1}$ crystal system with *Z* = 2 molecules per unit cell. The crystal structure of the compound shows the two methyl groups attached to the C11 atom are in a *gauche* conformation in relation to the C9 methylene group which in turn is antiperiplanar with respect to the C11 hydroxyl group. A similar disposition was observed for the C13 methyl group in relation to the C10 hydroxyl group. The most stable conformer obtained by conformational analysis shows the O3–H3 and O4–H4 hydroxyl groups in an *anti*-conformation. The differences observed between experimental and calculated results were interpreted in terms of intermolecular interactions in the crystal packing. The structure reveals that the crystal packing is governed by O–H \cdots O hydrogen bonding and weak C–H \cdots O and C–H \cdots π non-covalent interactions. A detailed analysis of Hirshfeld surfaces and their associated 2D fingerprint plots allowed quantifying the interactions within the crystal structures.

© 2020 Elsevier B.V. All rights reserved.

1. Introduction

Crystal engineering and supra-molecular chemistry are at the forefront of current structural chemistry research interest with a variety of applications related to the structure of different compounds [1,2]. Various non-covalent interactions, such as hydrogen bonding, halogen bonding, C–H \cdots π interactions, π -stacking and other weak forces, can be decisive in controlling the molecular

assembly in organic compounds and also play vital roles in various fields from medicinal chemistry to material science [3,4]. These interactions are individually weaker and geometrically less well-defined; however, their combined effect can be as important as strong interactions [5]. A proper understanding of these weak interactions is crucial to extrapolate structure-reactivity/property relationships [6]. Recently, we have reported the synthesis, spectroscopic characterization and a complete structural analysis of two Schiff bases, obtained from 4-aminoacetophenone, and their supra-molecular arrangement were studied by Hirshfeld surface analysis [7,8]. In addition, we have evaluated the role of the hydrogen bonds, halogen interactions and C–H \cdots π and π -stacking interactions that stabilize the crystal packing of a new perfluoromethylaminoenone

* Corresponding author.

E-mail address: dmgil@fbqf.unt.edu.ar (D.M. Gil).

¹ Member of the Research Career of CONICET.

derivative [9].

p-Hydroxyacetophenone and its derivatives are phenolic metabolites frequently found in both angiosperms and gymnosperms, where they have been considered to act as defense metabolites, mainly as antifungal agents [10–13]. On the other hand, prenylated *p*-hydroxyacetophenone derivatives have been proposed as biogenetic precursors of benzofurans and chromanes which are characteristic bioactive metabolites of certain tribes of the Asteraceae family [13–16]. In this sense, we recently described [17] a biomimetic synthesis of the natural benzofuran (**4**) and natural chromane (**3**) starting from the antifungal 4-hydroxy-3-(3-methyl-2-butenyl)-acetophenone (4-HMBA) (**1**) [10], the main secondary metabolite of *Senecio nutans* [18], *Xenophyllum poposum* [19], and *Xenophyllum incisum* [20]. These compounds were characterized by different spectroscopic techniques such as IR, Raman and UV–Vis and their crystal structures were solved by single-crystal XRD methods. Thus, treatment of (**1**) with *m*-chloroperbenzoic acid yielded a mixture of epoxide (**2**), along with the chromane 2,2-dimethyl-3-hydroxy-6-acetylchromane (**3**) and the benzofuran 10,11-dihydro-10-hydroxytremetone (**4**). Hydrolysis of epoxide (**2**) produced the phenol-diol 3-(2,3-dihydroxyisopentyl)-4-hydroxyacetophenone (**5**), a metabolite isolated from the medicinal plant *Werneria ciliolata* [21]. This phenol-glycol was isolated as an oil by preparative HPLC which crystallized after several weeks in the refrigerator producing single crystals suitable for structural studies. The results are presented and discussed here.

In this work, the synthesis and characterization of 3-(2,3-dihydroxy-isopentyl)-4-hydroxyacetophenone (**5**) is reported. The solid was characterized by IR, Raman and ¹H NMR spectroscopy. The crystal structure of the compound was solved by X-ray diffraction (XRD) methods along with the DFT calculations to study the molecular geometry. The role of weak hydrogen bonds and other intermolecular interactions in building possible supra-molecular assemblies was evaluated by Hirshfeld surface analysis.

2. Experimental

2.1. Synthesis of 3-(2,3-dihydroxy-isopentyl)-4-hydroxyacetophenone (racemic)

The compound was synthesized by treating of 4-hydroxy-3-(3-methyl-3-butenyl)-acetophenone (4-HMBA) with *m*-chloroperbenzoic acid as reported earlier [17]. During the formation of epoxide (**2**), an intramolecular nucleophilic attack by the phenolic hydroxyl at the epoxide carbons produces chromane (**3**) and benzofuran (**4**), while dissolution in aqueous solutions yields the corresponding solvolysis product, i.e. phenol-diol (**5**). After separation and purification by preparative HPLC phenol-diol (**5**) was obtained as colorless needles, m.p. 139–140 °C (from methanol). Single-crystals adequate for XRD measurements were obtained from slow evaporation of a methanolic solution of the compound at room temperature.

EIMS: *m/z* (rel. int. %) [M]⁺ 238 (4), 220 (5), 205 (2), 187 (2), 180 (18), 165 (6), 163 (7), 150 (25), 149 (29), 137 (52), 119 (12), 107 (21), 91 (11), 77 (16), 71 (17), 59 (39), 43 (100). ¹H NMR (200 MHz, CDCl₃): δ 7.79 *d* (1H, 2.1 Hz, H-6), 7.70 *dd* (1H, 8.3 and 2.1 Hz, H-4), 6.88 *d* (1H, 8.3 Hz, H-3), 3.90 *br* (3H, OH; this signal disappears by exchange with D₂O), 3.60 *dd* (1H, 10.3 and 1.4 Hz, H-10), 2.91 *dd* (1H, 14 and 1.4 Hz, H-9A), 2.66 *dd* (1H, 14 and 10.3 Hz, H-9B), 2.52 *s* (3H, H-8), 1.25 *s* and 1.23 *s* (3H each, H-12 and H-13) (for ¹H NMR in CD₃OD see Refs. [17]). The ¹H NMR spectrum in CDCl₃ is shown in Fig. S1 (Supplementary Information).

2.2. Instrumentation

¹H NMR spectra were recorded in CDCl₃ solvent on a Bruker AC (200 MHz) spectrometer. Tetramethylsilane (TMS) was used as internal standard. Chemical shifts were recorded in δ (ppm) values relative to TMS and *J* values were expressed in Hertz. Infrared absorption spectra were recorded in the range of 4000–400 cm⁻¹ on a PerkinElmer GX1 Fourier Transform infrared spectrometer with 2 cm⁻¹ of spectral resolution. The solid state Raman spectrum was measured at room temperature in the spectral range from 3500 to 50 cm⁻¹ using a ThermoScientific DXR Raman microscope. Raman data have been recorded using a diode-pump, solid state laser of 532 nm with a resolution of 5 cm⁻¹. The UV–Visible measurements were recorded using quartz cells (10 mm optical path length) in a Specord S-600 diode array spectrophotometer. For this purpose, a solution of 12.33 μg/L of compounds in ethanol was prepared. Each spectrum was recorded between 205 and 700 nm region.

2.3. X-ray diffraction data

The X-ray measurements were performed on an Oxford Gemini, Eos CCD diffractometer with graphite-monochromated CuKα (λ = 1.54184 Å) radiation. X-ray diffraction intensities were collected (ω scans with θ and κ-offsets), integrated and scaled with CrysAlisPro suite of programs [22]. The unit cell parameters were obtained by least-squares refinement (based on the angular settings for all collected reflections with intensities larger than seven times the standard deviation of measurement errors) using CrysAlisPro. Data were corrected empirically for absorption employing the multi-scan method implemented in CrysAlisPro. The structure was solved by intrinsic phasing with SHELXT of the SHELX suit of programs [23] and refined with SHELXL of the same package. All hydrogen atoms were located in a difference Fourier map phased on the heavier atoms and refined at their found positions with isotropic displacement parameters.

Crystal data and data collection procedure are summarized in Table 1. Crystallographic structural data have been deposited at the Cambridge Crystallographic Data Centre (CCDC). Enquiries for data can be direct to: Cambridge Crystallographic Data Centre, 12 Union Road, Cambridge, UK, CB2 1EZ or (e-mail) deposit@ccdc.cam.ac.uk or (fax) +44 (0) 1223 336033. Any request to the Cambridge Crystallographic Data Centre for this material should quote the full literature citation and the reference number CCDC 1958399.

2.4. Hirshfeld surface analysis

The Hirshfeld surface (HS) analysis and their decomposed two-dimensional fingerprint (FP) plots were used to quantify the contribution of intermolecular interactions that stabilize the crystal packing and to understand the nature of intermolecular interactions [24–27]. The HS and their 2D fingerprint plots were generated by using the CrystalExplorer17.5 program using the crystallographic information files (CIF) obtained from the X-ray crystal structure determination [28]. The function d_{norm} is given by the formula involving the ratio encompassing the distances of any surface point to the nearest interior (d_i) and exterior (d_e) atom and the van der Waals radii (r^{vdW}) of the atoms [24].

$$d_{norm} = \frac{d_i - r_i^{vdW}}{r_i^{vdW}} + \frac{d_e - r_e^{vdW}}{r_e^{vdW}} \quad (1)$$

The red regions in the d_{norm} plots indicate that the sum of d_e and d_i is shorter than the sum of van der Waals (vdW) radii and therefore considered to be a close contact. The white colour denotes intermolecular interactions with distances close to vdW contacts

Table 1
Crystal data and structure refinement for 3-(2,3-dihydroxy-isopentyl)-4-hydroxyacetophenone.

Empirical formula	
Formula weight	C ₁₃ H ₁₈ O ₄
Temperature	238.27
Wavelength	297(2) K
Crystal system	1.54184
Space group	Triclinic
Unit cell dimensions	$P\bar{1}$ $\alpha = 108.464(10)$ $\beta = 102.477(8)$ $\gamma = 102.324(7)$
Volume	a = 6.9478(5) Å b = 9.922(1) Å c = 10.928(1) Å
Z, density (calculated)	664.5(1) Å ³
Absorption coefficient	2, 1.191 Mg/m ³
F(000)	0.721 mm ⁻¹
Crystal size	256
θ -range for data collection	0.2020.354 mm ³
Index ranges	4.481–72.390°
Reflections collected	–8 ≤ h ≤ 6, –12 ≤ k ≤ 11, –13 ≤ l ≤ 13
Independent reflections	4270
Observed reflections [I > 2σ(I)]	2576 [R(int) = 0.0207]
Completeness to $\theta = 67.684^\circ$	1925
Refinement method	99.8%
Data/restraints/parameters	Full-matrix least-squares on F ²
Goodness-of-fit on F ²	2576/0/169
Final R indices ^a [I > 2σ(I)]	1042
R indices (all data)	R1 = 0.0491, wR2 = 0.1354
Largest diff. peak and hole	R1 = 0.0648, wR2 = 0.1515
	0.187 and –0.183 e.Å ⁻³

$$^a R_1 = \sum ||F_o| - |F_c|| / \sum |F_o|, wR_2 = [\sum w(|F_o|^2 - |F_c|^2)^2 / \sum w(|F_o|^2)^2]^{1/2}.$$

with d_{norm} equal to zero. The blue surfaces are assigned to contacts longer than the sum of vdW radii with positive d_{norm} values. The 3D d_{norm} surfaces were mapped over a fixed colour scale of –0.315 au (red) to 0.460 au (blue). The 2D fingerprint plot is the combination of d_i and d_e providing quantitative pictures of the intermolecular contacts, including the relative percentage of each type of interaction in the crystal. The FP plots were displayed by using a translated 0.6–2.6 Å range, and included reciprocal contacts.

Molecular electrostatic potential (ESPs) mapped over electron density distribution on 0.005 e Å⁻³ isosurfaces are calculated at B3LYP/cc-pVDZ approximation by using the TONTO program integrated into CrystalExplorer17.5.

2.5. Computational details

The quantum chemical calculations were performed using Gaussian 03 program package [29]. For structural optimization, the crystal structure geometry was used as a starting model. The molecular structure was fully optimized using B3LYP/6–311++G(d,p) level of theory. The vibration frequencies were calculated for the optimized structure in gas phase to ascertain the global minima on the potential energy surface and were found to have no imaginary frequencies. The assignment of the vibration modes and the potential energy distribution were calculated using the VEDA 4 program [30,31]. The UV–Visible electronic transitions have been calculated by using Time-dependent DFT (TD-DFT) approach [32] at B3LYP/6–311++G(d,p) level taking into account the solvent effect (ethanol) using the conductor-like polarizable continuum model (CPCM) [33].

3. Results and discussion

3.1. Conformational analysis and structural results

The potential energy curve for internal rotation around the C10–C11 bond calculated at B3LYP/6–311++G(d,p) approximation is shown in Fig. 1a. In this study we have selected the

C9–C10–C11–O4 dihedral angle because the conformation obtained in solid state is related with the mentioned angle (see below). The results of these calculations showed the existence of three conformers and the energies of CI and CIII conformers are significantly lower than CII conformer. The optimized molecular structures computed at B3LYP/6–311++G(d,p) level of the three conformers are depicted in Fig. 1b. Table S1 (Supplementary Information) shows the relative total energies and free energies of the three conformers calculated at the same level of theory. The frequencies calculated for the three structures were all positive confirming that they corresponds to minima in the potential energy curve.

In the most stable conformer for the compound (CI), the dihydroxy-isopentyl group adopts an *anti*-conformation, while in CII and CIII conformers, the O3–H2 and O4–H4 hydroxyl groups are present in a *gauche* conformation. In accordance with the results showed in Fig. 1b, CI is the most stable conformer, but it is not the conformer present in the crystal structure of the title compound (CII conformer). In the solid, the *gauche* conformation is mainly stabilized by intermolecular hydrogen bonding interactions (see below) that are absent in gas phase. The experimental and calculated geometrical parameters for the three possible conformers of 3-(2,3-dihydroxy-isopentyl)-4-hydroxyacetophenone are listed in Table 2.

3.2. Crystal structure

An ORTEP [34] diagram of the asymmetric unit content of the compound along with the atoms numbering scheme is shown in Fig. 2. The main experimental geometrical parameters are listed in Table 2, where the corresponding values obtained from quantum chemical calculations are also reported for comparison. There is a good agreement between both sets of structural data.

As expected from an extended π -bonding structure, the 4-hydroxyacetophenone ring is essentially planar with C8–C7–C5–C4 and C8–C7–C5–C6 dihedral angles of 176.4(2)° and –2.7(3)°, respectively. The overall molecular conformation can

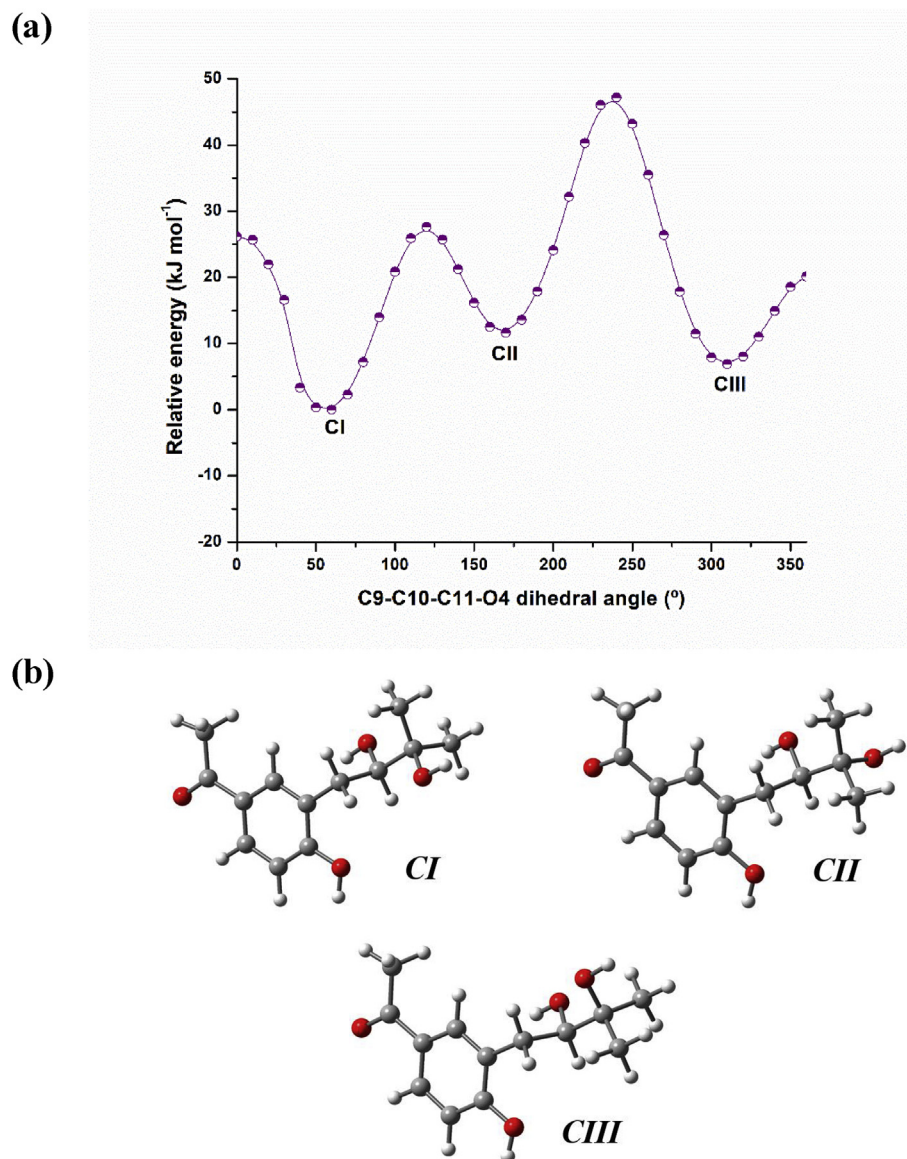


Fig. 1. (a) Potential energy curve around the C10–C11 bond computed at B3LYP/6–311++G(d,p) approximation; (b) Optimized molecular structures of the three possible conformations of 3-(2,3-dihydroxy-isopentyl)-4-hydroxyacetophenone.

be described by the relative orientation of the hydroxyl groups in the alkyl chain, which facilitate intermolecular hydrogen bonding. The torsion angle C1–C9–C10–C11 of $-160.56(14)^\circ$ shows an *anti*-conformation of the molecule about the C9–C10 bond. The hydroxyl bonded at C10 adopts a *gauche* conformation, with a torsion angle C1–C9–C10–O3 of $76.67(17)^\circ$. The optimized molecular structure of CII conformer (Fig. 1b) corroborates the *anti*-conformation of the dihydroxy-isopentyl chain with respect to the acetophenone core indicating that the calculations agree well with corresponding data from the X-ray structural studies. Observed bond lengths and angles agree with Organic Chemistry rules and with data reported for similar compounds [17,18]. The C–C bond lengths of the phenyl ring are in the range of 1.376(3)–1.400(3) Å, as expected for a resonant-bond structure. The carbonyl C=O bond length is equal to 1.221(3) Å, in agreement with the computed value (1.219 Å). The C(sp²)-O bond length is 1.350(2) Å, shorter than the other C(sp³)-O bond lengths [1.425(2) and 1.435(2) Å]. The dihydroxy-isopentyl moiety exhibits the expected tetrahedral bonding structure with C12–C11–C13 and C12–C11–O4 angles of

$111.71(17)^\circ$ and $108.37(16)^\circ$, respectively which is consistent with the sp³ hybrid character of C11 atom. A Newman projection of the C11–C10 bond shows that the two methyl groups attached to the C11 atom are in a *gauche* conformation in relation to the C9 methylene group which in turn is antiperiplanar with respect to the C11 hydroxyl group. A similar disposition was observed for the C13 methyl group in relation to the C10 hydroxyl group (see dihedral angles in Table 2). The small differences between the experimental and computed geometrical parameters can be attributed to the fact that theoretical calculations have been carried out with isolated molecules in gas phase whereas the experimental values correspond to the crystalline state, where intermolecular interactions play an important role.

The crystal packing in the title compound is stabilized mainly by O–H⋯O hydrogen bonding interactions (See Table 3, Fig. 3). In the structure, each molecule participates in four hydrogen bonds and these interactions dominate the crystal packing of the compound. As shown in Fig. 2a, neighbouring molecules are linked to each other through intermolecular O2–H2⋯O3 bonds. The polymeric

Table 2
Experimental and calculated bond lengths, angles and dihedral angles for the three possible conformations of 3-(2,3-dihydroxy-isopentyl)-4-hydroxyacetophenone.

Parameters ^a	Calculated ^b			Experimental ^c
	C1	C11	C111	
<i>Bond lengths (Å)</i>				
C1–C9	1.512	1.511	1.511	1.510(2)
C2–O2	1.363	1.369	1.365	1.350(2)
C9–C10	1.544	1.535	1.547	1.527(2)
C10–O3	1.426	1.425	1.424	1.425(2)
C10–C11	1.548	1.552	1.548	1.538(2)
C11–O4	1.436	1.451	1.435	1.435(2)
C11–C12	1.535	1.531	1.535	1.516(3)
C11–C13	1.535	1.532	1.538	1.518(3)
C5–C7	1.494	1.494	1.494	1.477(3)
C7–O1	1.223	1.219	1.220	1.221(2)
C7–C8	1.521	1.519	1.520	1.488(3)
<i>Bond angles (°)</i>				
C5–C7–C8	118.9	118.9	118.9	120.41(18)
C1–C9–C10	112.0	112.7	112.3	111.08(13)
C9–C10–C11	113.9	114.8	113.1	113.80(13)
C10–C11–O4	104.1	102.0	106.2	104.43(12)
C10–C11–C12	112.3	112.8	110.2	112.79(15)
C10–C11–C13	109.5	111.6	110.7	110.11(15)
C9–C10–O3	111.4	106.9	110.5	107.49(13)
<i>Dihedral angles (°)</i>				
C1–C9–C10–C11	–179.4	–168.6	178.8	–160.56(14)
C1–C9–C10–O3	59.99	68.65	57.17	76.67(17)
C9–C10–C11–O4	56.40	–175.0	–50.74	–174.44(14)
C9–C10–C11–C12	–62.98	–57.73	–169.7	–57.0(2)
C9–C10–C11–C13	173.7	68.92	68.08	68.5(2)

^a See Fig. 2 for atoms numbering scheme.

^b Calculated values at B3LYP/6–311++G(d,p) level of theory.

^c Experimental values obtained from single crystal XRD data.

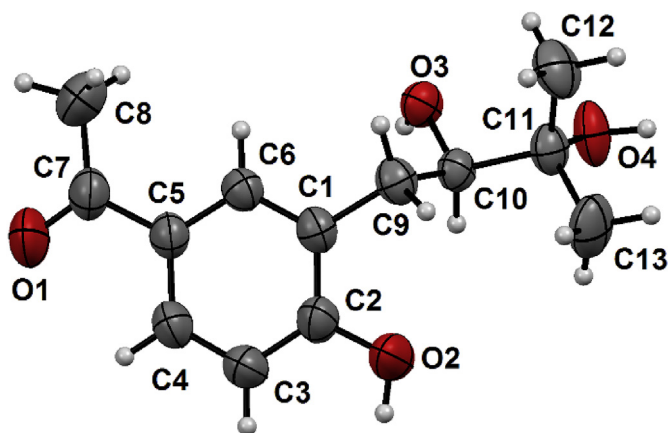


Fig. 2. ORTEP diagram of the asymmetric unit of 3-(2,3-dihydroxy-isopentyl)-4-hydroxyacetophenone, showing the labelling of the non-hydrogen atoms. Ellipsoids are drawn at the 30% probability level.

Table 3
Hydrogen bonds parameters (Å, °) for 3-(2,3-dihydroxy-isopentyl)-4-hydroxyacetophenone.

D–H...A	D–H	H...A	D...A	< D–H...A	Label in Fig. 5
C12–H12C...O2 ^{#1}	0.96	2.62	3.539(3)	160.8	4
O2–H2...O3 ^{#2}	0.89(3)	1.77(3)	2.654(2)	169(3)	2
O3–H3...O4 ^{#3}	0.86(3)	1.79(3)	2.642(2)	171(2)	3
O4–H4...O1 ^{#4}	0.86(3)	1.92(3)	2.768(2)	171(3)	1

Symmetry transformations used to generate equivalent atoms: (#1) $x-1, y, z$; (#2) $x+1, y, z$; (#3) $-x, -y, -z+1$; (#4) $x-1, y-1, z-1$.

chains are further linked via intermolecular O4–H4...O1(keto) hydrogen bonds, thus forming a $R_4^4(30)$ synthon. The rings are

edge-fused to generate a two-dimensional molecular assembly as shown in Fig. 3a. In addition, to molecules are also linked via non-classical C13–H13C...O1 hydrogen bonds [$d(O1...H13C) = 2.793$ Å]. In the crystal packing of the title compound, the oxygen atom O3 from the hydroxyl group participates in intermolecular O3–H3...O4 hydrogen bonding interactions forming inversion dimers with $R_2^2(10)$ graph-set ring motif, as shown in Fig. 3b. Two molecules are also linked through the H12C hydrogen of the methyl group in the dihydroxy-isopentyl moiety and hydroxyl oxygen atom O2 to form C12–H12...O2 intermolecular interactions [$d(C-H...O) = 2.62$ Å, $\angle(C-H...O) = 160.8^\circ$]. The supra-molecular arrangement of the title compound is further controlled by C–H... π interactions (Fig. 4) involving the H9 hydrogen of the methylene group and the C1–C6 benzene ring [centroid Cg1; symmetry 1-x, 1-y, 1-z].

3.3. Hirshfeld surface analysis

The intermolecular interactions affecting the packing modes of the title compound are more easily understood using Hirshfeld surface, with the results further highlighting the power of this technique in mapping out interactions. It is well-known that the Hirshfeld surface analysis is a useful visualization tool for the analysis of intermolecular interactions in the crystal packing and the fingerprint plots is also used to quantify the contribution of various intermolecular contacts present in the crystal structures. The HS are illustrated in Fig. 5 showing surfaces that have been mapped with d_{norm} property. The 2D fingerprint plot provides a quantitative description of all the intermolecular interactions in the crystal (Fig. 6). The FP plots can be decomposed to highlight particular atoms pair close contacts. This decomposition enables separation of the contributions from different interactions, which overlap in the full FP plot. In general, the intermolecular interactions play a crucial role in the crystal structures of the studied compound. A close examination of the FP plots generated for the title compound indicates that the non-directional H...H interactions are predominant (see Fig. 6) and comprise 60.9% of the total HS area of the molecule, having minimum value of ($d_e + d_i$) of 2.40 Å. These interactions play a major role in the strength of the crystal lattice and simply represent regions which are dominated by dispersion interactions [35]. The proportion of H...H contacts can be used as reference for the effectiveness and stability of the crystal packing and the relevance of another contacts can be referred to this standard [35]. H...H contacts are weaker than other interactions, and it is not clear if they are attractive or repulsive in nature even though H...H bond paths are commonly found [36]. The dominant interactions between the hydroxyl O4–H4 and the O1 atom from the carbonyl group are observed in the HS as the bright red areas marked as 1 in Fig. 5. The red spots labelled as 2 are assigned to O2–H2...O3 hydrogen bonding interactions. These interactions are the major contributor of the $R_4^4(30)$ supramolecular synthon. The visible spots around the hydroxyl O4–H4 (labelled as 3) are attributed to O3–H3...O4 contacts. The O...H/H...O contacts appear as distinct sharp spikes on the FP plots, with a minimum value ($d_e + d_i$) of 1.65 Å coming from the strongest O3–H2...O3 and O3–H3...O4 contacts, in accordance with the geometrical parameters reported in Table 3. The light red spots, labelled as 4 in the back view of HS showing in Fig. 5, are due to non-classical C–H...O hydrogen bonds involving as acceptor the O2 from the hydroxyl group of one molecule and as donor the methyl group of the isopentyl moiety of another molecule. The weak C13–H13C...O1 interactions are not visible in the Hirshfeld surfaces because the distances are longer than the sum of vdW radii. In the FP plot, they appear as a thickening of the sharp spikes around ($d_e + d_i$) of 2.6 Å,

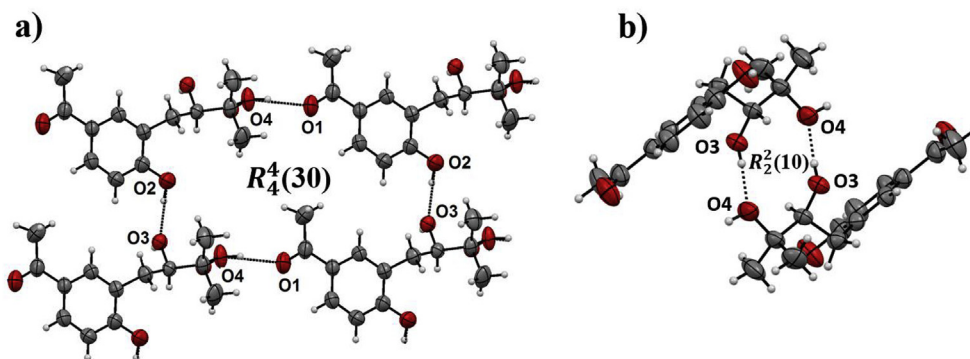


Fig. 3. Molecular packing of 3-(2,3-dihydroxy-isopentyl)-4-hydroxyacetophenone showing the formation of two-dimensional supra-molecular assemblies.

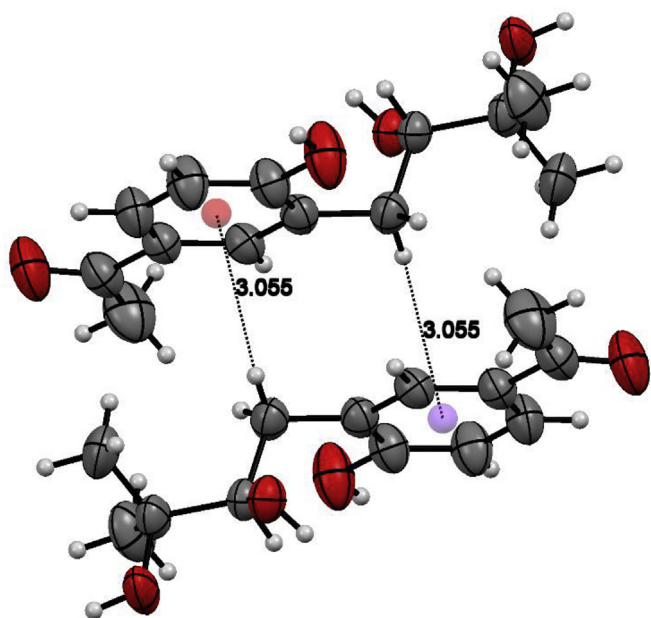


Fig. 4. View of the crystal packing of 3-(2,3-dihydroxy-isopentyl)-4-hydroxyacetophenone showing C–H \cdots π interactions.

in accordance with the values reported in Table 3. The proportion of the O \cdots H/H \cdots O interactions, calculated from the decomposition of the FP plot, is 23.3% of the total Hirshfeld surfaces of the molecule. Besides, the decomposition of the FP plot shows that C \cdots H/H \cdots C contacts comprise 14.6% of the total HS area of the molecule. They correspond to all the C–H \cdots π interactions, which appear in the FP plot in a characteristic manner.

We have computed the molecular electrostatic potential (ESP) mapped on electron density isosurface in order to study the attractive character of intermolecular hydrogen bonds which stabilize the crystal packing of the title compound. The Hirshfeld surface mapped over the electrostatic potential for 3-(2,3-dihydroxy-isopentyl)-4-hydroxyacetophenone is shown in Fig. 7. The blue and red colours are attributed to positive and negative regions, respectively. The ESP shows the highest electropositive value of +0.2503 a.u. near the H2 atom attached to strong O2 donor, and a strong electronegative region (−0.0896 a.u.) is found around the O3 atom. This favours the formation of the strongest O2–H2 \cdots O3 hydrogen bonds, as described in Table 3. In addition, we have observed a positive region located around the H3 atom (+0.2149 a.u.) and a negative part located at the O4 atom of the

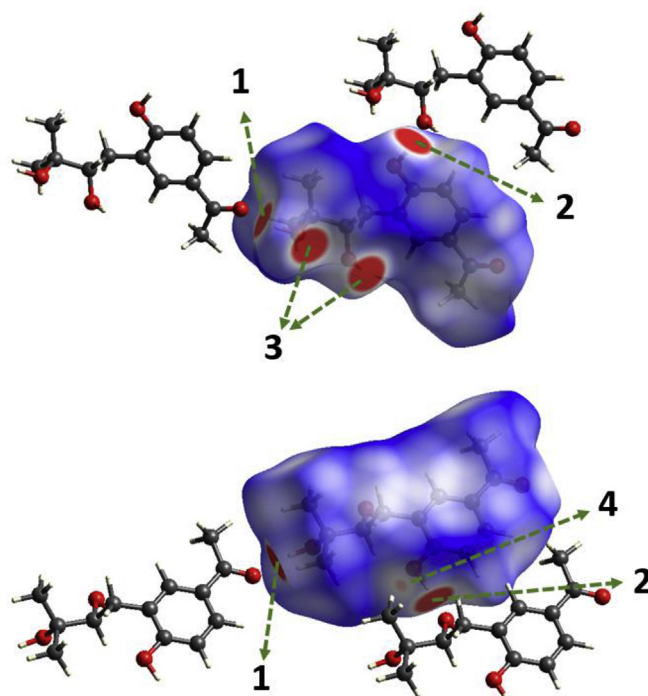


Fig. 5. Front and back views of the Hirshfeld surfaces mapped with d_{norm} property. Labels are discussed in the text and in Table 3.

hydroxyl group (−0.080 a.u.). Therefore, from an electrostatic point of view, the interaction between both groups is favoured forming O3–H3 \cdots O4 hydrogen bonds. Finally, the ESP values at the O1 and H4 atoms are the smallest (−0.0542 and +0.1692 au, respectively). These results indicate that the interaction O4–H4 \cdots O1 is weaker, in accordance with the results reported in Table 3. The lowest ESP value at the O2 atom showed in Figs. 7 (−0.0195 a.u.) is an indicator of the weak C12–H12C \cdots O2 hydrogen bond (Table 3, Fig. 4).

3.4. Vibrational results

Fig. 8 depicts the experimental FTIR and Raman spectra of 3-(2,3-dihydroxy-isopentyl)-4-hydroxyacetophenone in solid state. The frequencies obtained theoretically corresponds to CII conformer which is the structure present in solid state. The observed and computed vibration frequencies, together with the corresponding assignment of bands, are listed in Table 4. A tentative assignment of the observed bands has been performed by

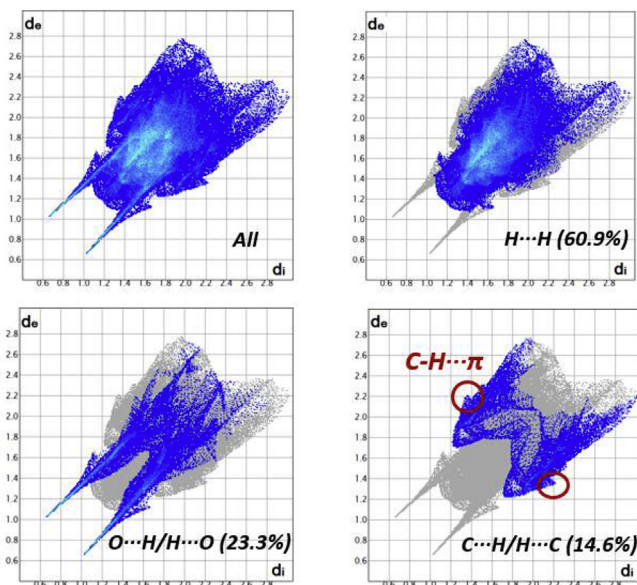


Fig. 6. Fingerprint plots of the title compound: full and resolved into H...H, O...H/H...O and C...H/H...C contacts showing the percentages of contacts contributing to the total HS area.

comparison with theoretical mode frequencies. In this work, a scale factor 0.9679 was used to counterbalance the systematic errors caused by basis set incompleteness, neglect of electron correlation and vibrational anharmonicity [37,38]. Very good agreement between the experimental and computed vibrational data supported the proposed assignment. A comparison between the experimental and theoretical IR and Raman spectra calculated at B3LYP/6-311++G(d,p) approximation is shown Figs. S2 and S3 (Supplementary Information).

3.4.1. OH vibrations

The vibrations of hydroxyl group show variation according to the molecular environment. Generally, free hydroxyl groups without hydrogen bonding interactions show IR absorption bands between 3700 and 3500 cm^{-1} . For the title compound, the O–H

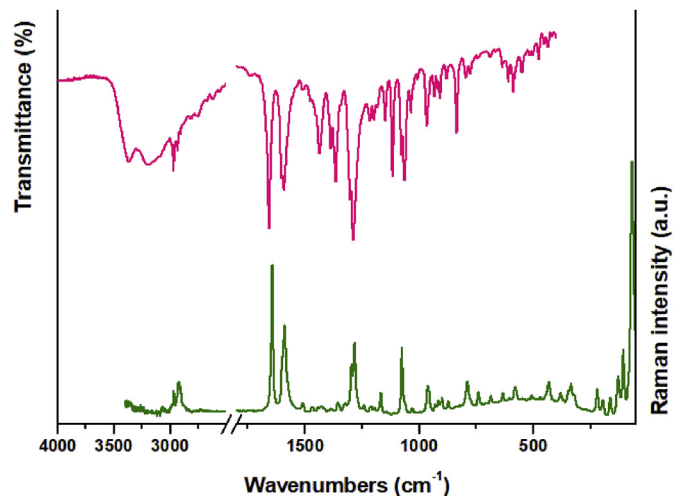


Fig. 8. IR and Raman spectra of 3-(2,3-dihydroxy-isopentyl)-4-hydroxyacetophenone in solid state.

stretching modes appear as broad bands between 3370 and 3200 cm^{-1} hence indicating that all hydroxyl groups are involved in intermolecular hydrogen bonds as was deduced from the crystal structure, in accordance with related compounds [39,40].

The bands located at 1364, 1302, 1198 and 1116 cm^{-1} in the IR spectrum (1357, 1296 and 1195 cm^{-1} in Raman) are assigned to C–O–H bending modes. These values are in agreement with the computed wavenumbers (see Table 4). The torsion OH modes are assigned to the bands at 365 and 221 cm^{-1} in the Raman spectrum.

3.4.2. CH₃ and CH₂ group vibrations

The methyl groups generate bands at 2986 and 2971 cm^{-1} in the IR spectrum (2985 and 2969 cm^{-1} in Raman) which are assigned to CH₃ antisymmetric stretching mode. The bands corresponding to the CH₃ symmetric stretching mode appear at 2933 cm^{-1} in IR with counterparts in Raman at 2928 and 2920 cm^{-1} . The bands located at 1476 and 1453 cm^{-1} (1468 and 1442 cm^{-1} in Raman) are assigned to the antisymmetric CH₃ bending mode of the methyl groups from the isopentyl moiety. The Raman band at 1426 cm^{-1} is

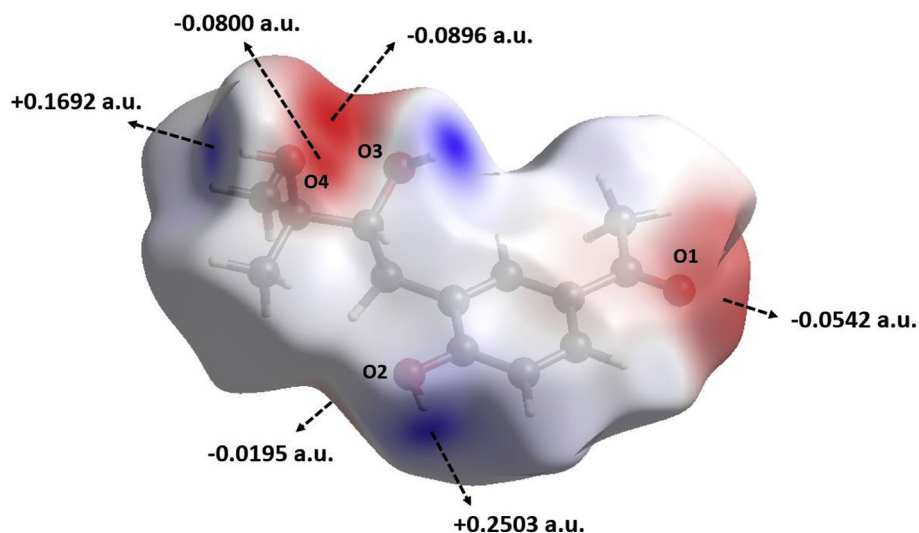


Fig. 7. Hirshfeld surface mapped over the calculated electrostatic potential in the range -0.0910 (red) to $+0.2524$ (blue) atomic units for 3-(2,3-dihydroxy-isopentyl)-4-hydroxyacetophenone.

Table 4
Selected experimental and theoretical vibration frequencies (cm^{-1}) and their tentative assignments for CII conformer of 3-(2,3-dihydroxy-isopentyl)-4-hydroxyacetophenone.

IR (solid)	Raman (solid)	Calculated		Assignment of modes (PED \geq 10%) ^c
		Unscaled ^a	Scaled ^b	
3370	—	3832	3709	ν O–H (100)
3200	—	3793	3671	ν O–H (100)
3085	3077	3195	3092	ν C–H (99)
3056	—	3147	3046	ν C–H (84)
2986	2985	3091	2992	ν_a CH ₃ CO (99)
2971	2969	3084	2985	ν_a CH ₃ -IP (73)
2965	2962	3057	2959	ν_s CH ₂ (100)
2933	2928	3034	2936	ν_s CH ₃ CO (100)
—	2920	3023	2926	ν_s CH ₃ -IP (91)
2911	2907	2997	2901	ν C10–H (93)
1655	1643	1735	1679	ν C=O (87)
1602	1598	1644	1591	ν CC-R (64)
1592	1588	1627	1575	ν CC-R (50)
1511	1510	1533	1484	δ CCH-R (44) + δ CCC-R (16)
1476	1468	1511	1462	δ_a CH ₃ -IP (79)
1453	—	1501	1452	δ_a CH ₃ -IP (82)
—	1442	1490	1442	δ_a CH ₃ -IP (62)
1434	1434	1478	1431	δ CH ₂ (67)
—	1426	1472	1425	δ_a CH ₃ CO (94)
1386	1387	1451	1404	ν CC-R (47) + δ CCH (10)
1364	1357	1426	1380	ν C9–C10 (36) + δ C10–OH (19) + δ CCH (12)
1343	1346	1386	1342	δ_s CH ₃ CO (86)
—	1324	1368	1324	ν CC-R (20) + δ C–O2–H (11)
1302	1296	1310	1267	δ C9–C10–H (12) + δ C10–OH (12)
1289	1284	1291	1250	ν C2–O2 (49)
—	1242	1278	1237	ν C5–C7 (22)
1215	1209	1227	1188	δ CCH-R (23)
1198	1195	1207	1168	δ C–O2–H (21) + $\tau\omega$ CH ₂ (11)
1183	1167	1180	1142	δ CCH-R (44) + δ C–O2–H (14)
1148	1143	1169	1131	ρ CH ₃ (29)
1116	—	1130	1094	δ C–O4–H (41) + ρ CH ₃ (12)
1078	1074	1098	1063	ν C10–O3 (26)
1064	1062	1077	1042	ν C10–O3 (26) + δ CCH-R (16)
1035	—	1042	1009	ρ CH ₃ (70) + γ C=O (22)
—	1030	1033	999	ρ CH ₂ (24) + ν C9–C10 (15)
1006	—	1012	980	ρ CH ₃ -IP (32)
966	962	976	945	ν C10–C11 (20) + ρ CH ₃ -IP (17)
934	928	969	938	γ CCH-R (83)
920	916	961	930	ρ CH ₃ -CO (44) + ν C7–C8 (25)
909	908	931	901	ρ CH ₃ -IP (39)
—	898	927	897	ν C1–C9 (17) + γ CCH-R (15) + δ CCC-R (11)
880	—	915	886	γ CCH-R (27) + ν CC-R (10)
—	873	904	875	γ CCH-R (29) + ν C11–O4 (10)
836	—	879	851	ν C9–C10 (30) + ρ CH ₂ (16)
796	790	825	799	γ CCH-R (83)
776	—	804	778	ν_s C(CH ₃) ₂ (21)
743	741	776	751	δ CCC-R (20)
723	—	746	722	γ CCC-R (51)
689	685	693	671	ν C7–C5 (38) + δ CCC-R (17) + ν CC-R (11)
635	634	642	621	γ C=O (21)
608	604	614	594	δ CCC-R (31)
588	580	590	571	δ CC=O (35) + ν C7–C8 (11)
551	549	571	553	ν_s C(CH ₃) ₂ (14) + δ C10–C11–C13 (13)
515	—	543	526	γ CCC-R (29)
501	507	512	496	γ CCC-R (41)
477	471	494	478	δ O2–C2–C3 (70)
454	—	475	460	τ O3–H (51)
420	—	424	410	δ C13–C20–O4 (31) + ρ CH ₂ (12)
—	380	413	400	δ C8–C7–C5 (49)
—	365	372	360	τ O2–H (89)
—	346	356	345	δ C9–C10–O3 (41)
—	335	345	334	δ C(CH ₃) ₂ (55)
—	322	340	329	ν CC-R (28) + δ CCC-R (24) + δ C8–C=O (21)
—	221	238	230	τ O4–H (52) + τ CH ₃ -IP (10)
—	196	204	197	δ C19–C10–C11 (29) + τ CCCC-R (20)
—	164	156	151	τ CH ₃ -CO (93)
—	129	151	146	δ C7–C5–C6 (35) + δ C9–C10–C11 (21)
—	107	108	105	τ CCCC-R (75)

Table 4 (continued)

IR (solid)	Raman (solid)	Calculated		Assignment of modes (PED \geq 10%) ^c
		Unscaled ^a	Scaled ^b	
–	68	71	69	τ C8–C7–C5–C6 (61)

^a Calculated vibration frequencies at B3LYP/6–311++G(d,p) level of theory.

^b Scale factor used 0.9679.

^c ν : stretching, δ : bending, γ : out-of-plane bending, ρ : rocking, τ : torsion modes; s: symmetric, a: antisymmetric; R: ring; IP: isopentyl group.

assigned to the antisymmetric CH₃ stretching mode of the acetyl group. These assignments are in agreement with reported data in literature [17,18] and with the calculated values (see Table 4). The IR absorption band at 1343 cm⁻¹ is assigned to symmetric CH₃ bending mode corresponding to the methyl group attached to the C=O moiety. The title molecule contains one methylene group. The IR absorption band at 2965 cm⁻¹ is assigned to the CH₂ symmetric stretching mode, which agrees well with the computed value at 2959 cm⁻¹ (scaled value). The CH₂ bending mode is associated with the IR and Raman bands observed at 1434 cm⁻¹, in agreement with the calculated value (1431 cm⁻¹).

3.4.3. C–H vibrations

The aromatic C–H stretching modes generate multiple bands in the region 3100–3000 cm⁻¹ [41]. For the title compound, the IR absorption bands observed at 3085 and 3056 cm⁻¹ (3077 cm⁻¹ in Raman) are assigned to C–H stretching mode of the phenyl ring. These results are in accordance with the computed values (see Table 4) and with reported values for similar compounds [39–44]. The bands corresponding to the C–H in-plane bending vibrations appear in the 1350–1000 cm⁻¹ range [39–44] and usually appear mixed with C–C stretching modes. For the title compound, the IR bands at 1215 and 1183 cm⁻¹, with counterparts in Raman at 1209 and 1167 cm⁻¹ are attributed to C–H in-plane bending modes. The bands located at 934, 880 and 796 cm⁻¹ in the IR spectrum (928, 873 and 790 cm⁻¹ in Raman) are assigned to C–H out-of-plane bending modes.

3.4.4. Skeletal vibrations

The C=O stretching mode is very sensitive to intra and intermolecular interactions. The observed band at 1655 cm⁻¹ in the IR spectrum, with counterpart in Raman at 1643 cm⁻¹, reflects that the C=O group is involved in the formation of a dimer via C=O...H hydrogen bonding interactions, as was deduced from the crystal structure. These results are in agreement with the computed value (1679 cm⁻¹) and with the values previously reported for similar compounds [30–45], in which the C=O group is involved in intramolecular hydrogen bonds. The C–C stretching modes of the alkyl chain produce bands at 966, 836, 776 and 689 cm⁻¹ in the IR spectrum and at 1242, 962, 898 and 685 cm⁻¹ in Raman. In the region between 1600 and 1300 cm⁻¹ the characteristic signals attributed to the C–C stretching modes of the phenyl ring, are observed in both, the IR and Raman spectra (see Table 4). The IR

spectrum shows strong absorptions at 1289, 1078 and 1064 cm⁻¹, with Raman counterparts at 1284, 1074 and 1062 cm⁻¹, which are attributed to C–O stretching modes.

3.5. Electronic spectra

The electronic spectrum for the title compound was calculated in ethanol as solvent at B3LYP/6–311++G(d,p) approximation. The observed and calculated electronic transitions of high oscillator strengths are listed in Table 5. The comparison between experimental and computed UV–visible spectra of 3-(2,3-dihydroxy-isopentyl)-4-hydroxyacetophenone is shown in Fig. 9. The low intensity band at 224 nm in the experimental spectra is assigned to HOMO-1 to LUMO+1 electronic transition, in accordance with the computed value (217 nm). The sharp and strong absorption band at 278 nm, matches well with the calculated value at 270 nm and arises mainly from HOMO to LUMO excitation and contains contributions from electronic transition among HOMO-2 \rightarrow LUMO orbitals. The shoulder observed at 263 nm in the experimental spectrum (calculated: 258 nm, $f = 0.1153$) is mainly attributed to transition from HOMO-2 \rightarrow LUMO and HOMO \rightarrow LUMO+1 orbitals. The HOMO corresponds to a p -type orbital character over the oxygen atoms from the carbonyl and hydroxyl groups and a π bonding system localized over phenyl ring (see Fig. 9). The LUMO has also π symmetry localized over the same moieties. The band gap between HOMO and LUMO frontier molecular orbitals is a very useful parameter which determines the chemical reactivity of molecules [46,47]. For the title molecule, the computed HOMO–LUMO energy gap in ethanol as solvent was found to be 3.645 eV. This strong HOMO to LUMO interaction results in intramolecular charge transfer band in the electronic absorption spectrum.

3.6. NBO analysis

The Natural Bond Orbital (NBO) analysis is an important tool for interpretation of intra and intermolecular interactions and also provides a convenient basis for investigating charge transfer or hyperconjugative interactions in different molecular systems. The larger value of $E^{(2)}$ (interaction energy) indicates the more donating tendency from electron donors to electron acceptors [48]. NBO analysis has been performed for the three possible conformations of the title compound at B3LYP/6–311++G(d,p) approximation. The results of second-order perturbation theory analysis of the Fock

Table 5

Experimental and calculated absorption wavelengths and oscillator strength for 3-(2,3-dihydroxy-isopentyl)-4-hydroxyacetophenone.

Wavelength (nm)		Oscillator strength	Assignment
Experimental	Calculated		
224	217	0.0025	HOMO-1 \rightarrow LUMO +1 (100%)
263 s h	258	0.1153	HOMO-2 \rightarrow LUMO (57%) HOMO \rightarrow LUMO (17%)
278	270	0.2299	HOMO \rightarrow LUMO+1 (23%) HOMO \rightarrow LUMO (80%) HOMO-2 \rightarrow LUMO (13%)

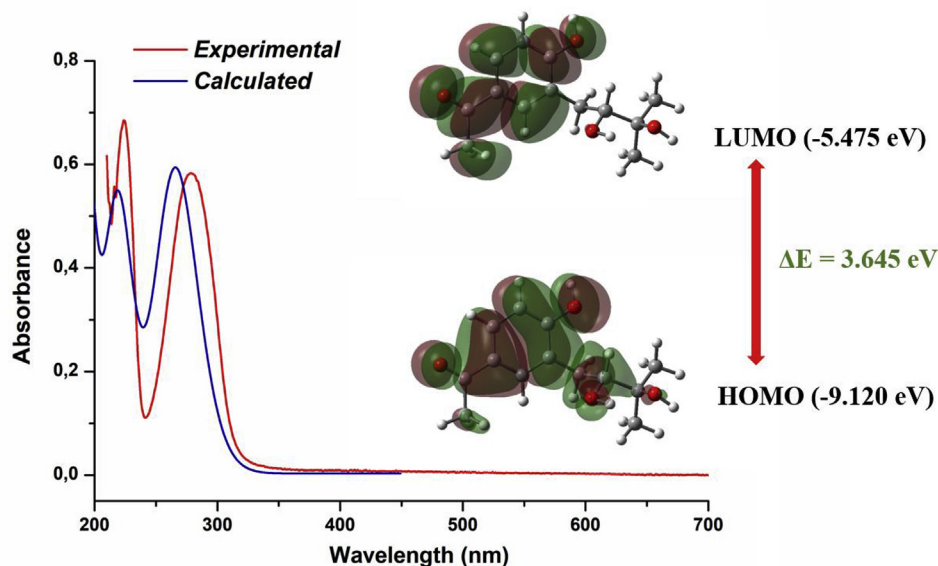


Fig. 9. Comparison between experimental and computed UV–Vis spectra for 3-(2,3-dihydroxy-isopentyl)-4-hydroxyacetophenone. HOMO and LUMO frontier molecular orbitals with their corresponding energies are also given.

Table 6

Second-order perturbation theory analysis of the Fock matrix for 3-(2,3-dihydroxy-isopentyl)-4-hydroxyacetophenone calculated by NBO approach at B3LYP/6-311++G(d,p) level of theory.

Interaction ^a	E ⁽²⁾ ^b		
	C _I	C _{II}	C _{III}
LP O1 → σ* C7–C8	90.58	90.29	87.95
LP O1 → σ* C5–C7	90.20	90.49	90.37
LP O2 → π* C2–C3	126.0	148.7	148.3
LP O3 → σ* C9–C10	32.73	35.65	31.81
LP O4 → σ* C11–C12	29.42	27.50	32.10
LP O4 → σ* C11–C13	30.22	31.18	27.71

^a LP denotes lone pair on the specified atom. See Fig. 2 for atoms numbering scheme.

^b Energy values in kJ mol⁻¹.

matrix are listed in Table 6.

The lone pair of O1 oxygen donates its electrons to the σ-type anti-bonding orbitals σ* C7–C8 and σ* C5–C7 with stabilization energies in the ranges 87.95–90.58 and 90.20–90.49 kJ mol⁻¹, respectively. The interaction between the LP O2 and the π* C2–C3 gives more stabilization of the molecule in the three possible conformation being more relevant in C_{II} and C_{III} conformers. This interaction is an indicative of the double bond character of the C2–O2.

4. Conclusions

The compound 3-(2,3-dihydroxy-isopentyl)-4-hydroxyacetophenone was synthesized and characterized by ¹H NMR, IR, Raman and UV–visible spectroscopies. The crystal structure has been elucidated by single crystal X-ray diffraction methods. The substance crystallizes in the triclinic $P\bar{1}$ crystal system with $Z = 2$ molecules per unit cell. The structure reveals weak non covalent contacts along with hydrogen bonding interactions that form the supra-molecular assembly. A detailed exploration of the intermolecular interactions that stabilize the crystal packing has been evaluated by using the Hirshfeld surface analysis and their associated 2D fingerprint plots. These results reveal that the crystal

packing is stabilized by O2–H2···O3, O3–H3···O4 and O4–H4···O1 hydrogen bonds. In addition, the supra-molecular packing were also stabilized by weak C–H···O and C–H···π and interactions. The molecular structure of the title compound was optimized and the vibrational wavenumbers were determined theoretically and the normal modes of vibration were assigned by using the potential energy distribution (PED) analysis. TD-DFT calculations have been performed to assign the electronic transitions showing a very good agreement with the observed UV–Visible spectrum.

Credit author statement

Diego M. Gil: Conceptualization, Investigation, writing-original draft preparation, writing-review and editing. Emilio Lizarraga: Synthesis of the compound and analysis of NMR spectra. Gustavo A. Echeverría and Oscar E. Piro: Crystal structure determination and Formal analysis. César A.N. Catalán: Analysis of NMR spectra, writing-review and editing.

Declaration of competing interest

The authors declare no conflicts of interest.

Acknowledgments

The authors thank ANPCyT (PICT 2016–0226) and SCAIT (Project D639/2), CONICET (PIP 11220130100651CO) and UNLP (Grant to Project 11/X857) of Argentina for financial support. G.A.E., D.M.G. and O.E.P are research fellows of CONICET.

Appendix A. Supplementary data

Supplementary data to this article can be found online at <https://doi.org/10.1016/j.molstruc.2020.128393>.

References

- [1] G.R. Desiraju, *The Crystal as a Supramolecular Entity*, John Wiley & sons, Chichester, 1996.
- [2] Z. Setifi, D. Zambon, F. Setifi, M. El-Ghozzi, R. Mahiou, C. Glidewell, *Acta*

- Crystallogr. C73 (2017) 674–681.
- [3] M. Joy, N. Alex, J.J. Malayan, C. Sudarsanakumar, A. Mathews, *Chemistry* 1 (2016) 5974–5981.
- [4] P.A. Raffo, S. Suárez, A.C. Fantoni, R. Baggio, F.D. Cukiernik, *Acta Crystallogr. C73* (2017) 667–673.
- [5] R. Banerjee, G.R. Desiraju, R. Mondal, J.A.K. Howard, *Chem. Eur J.* 10 (2004) 3373–3383.
- [6] B. Mathew, A.A. Adeniyi, S. Dev, M. Joy, G. Uçar, G.E. Mathew, A. Singh-Pillay, M.E.S. Soliman, *J. Phys. Chem. B* 121 (2017) 1186–1203.
- [7] M. Rocha, A. Di Santo, G.A. Echeverría, O.E. Piro, F.D. Cukiernik, S.E. Ulic, D.M. Gil, *J. Mol. Struct.* 1133 (2017) 24–36.
- [8] D.M. Gil, F.F. Salomón, G.A. Echeverría, O.E. Piro, H. Pérez, A. Ben Altabef, *Spectrochim. Acta* 185 (2017) 286–297.
- [9] M. Rocha, D.M. Gil, G.A. Echeverría, O.E. Piro, J.J. Jios, S.E. Ulic, *J. Fluor. Chem.* 208 (2018) 36–47.
- [10] J.R. Soberón, E.F. Lizarraga, M.A. Sgariglia, M.B. Carrasco Juárez, D.A. Sampietro, A. Ben Altabef, C.A.N. Catalán, M.A. Vattuone, Antonie van Leeuwenhoek Journal of Microbiology 108 (2015) 1047–1057.
- [11] A. Mendes do Nascimento, M.J. Salvador, R.C. Candido, S. de Albuquerque, D.C.R. de Oliveira, *J. Pharm. Pharmacol.* 56 (2004) 663–669.
- [12] G.J. Parent, I. Giguère, M. Mageroy, J. Bohlmann, J.J. MacKay, *Plant Cell Environ.* 41 (2018) 620–629.
- [13] Y. Zhao, C.-A. Geng, H. Chen, Y.-B. Ma, X.-Y. Huang, T.-W. Cao, K. He, H. Wang, X.-M. Zhang, J.-J. Chen, *Bioorg. Med. Chem. Lett* 25 (2015) 1509–1514.
- [14] P. Proksch, E. Rodriguez, *Phytochemistry (Oxf.)* 22 (1983) 2335–2348.
- [15] L. Margl, C. Ettenhuber, I. Gyurján, M.H. Zenk, A. Bacher, W. Eisenreich, *Phytochemistry (Oxf.)* 66 (2005) 887–899.
- [16] R. Siebertz, P. Proksch, V. Wraytand, L. Witte, *Phytochemistry (Oxf.)* 28 (1989) 789–793.
- [17] D.M. Gil, E. Lizarraga, G.A. Echeverría, O.E. Piro, C.A.N. Catalán, A. Ben Altabef, *J. Mol. Struct.* 1146 (2017) 164–178.
- [18] E. Lizarraga, D.M. Gil, G.A. Echeverría, O.E. Piro, C.A.N. Catalán, A. Ben Altabef, *Spectrochim. Acta* 127 (2014) 74–84.
- [19] A.M. González, M.I. Tracanna, S.M. Amani, C. Schuff, M.J. Poch, H. Bach, C.A.N. Catalán, *Nat. Prod. Commun.* 7 (2012) 1663–1666.
- [20] M.J.A. de Marchese, C.S. de Heluani, C.A.N. Catalán, C.A. Griffin, J.B. Vaughn Jr., W. Herz, *Biochem. Systemat. Ecol.* 35 (2007) 169–175.
- [21] S. Piacente, R. Aquino, N. de Tommasi, O. Lock de Ugaz, H. Chavez Orellana, *Phytochemistry (Oxf.)* 31 (1992) 2182–2184.
- [22] CrysAlisPro, Oxford diffraction Ltd., version 1.171.33.48 (release 15-09-2009 CrysAlis171.NET).....
- [23] G.M. Sheldrick, *Acta Crystallogr. A* 64 (2008) 112–122.
- [24] J.J. McKinnon, M.A. Spackman, A.S. Mitchell, *Acta Crystallogr. B* 60 (2004) 627–668.
- [25] J.J. McKinnon, D. Jayatilaka, M.A. Spackman, *Chem. Commun.* (2007) 3814–3816.
- [26] M.A. Spackman, D. Jayatilaka, *CrystEngComm* 11 (2009) 19–32.
- [27] M.A. Spackman, *Chem. Rev.* 92 (2002) 1769–1797.
- [28] M.J. Turner, J.J. McKinnon, S.K. Wolff, D.J. Grimwood, P.R. Spackman, D. Jayatilaka, M.A. Spackman, *CrystalExplorer17* (2017). University of western Australia. <http://hirshfeldsurface.net>.
- [29] M.J. Frisch, J.A. Pople, J.S. Binkley, *J. Chem. Phys.* 80, 3265 (1984). M.J. Frisch, G.W. Trucks, H.B. Schlegel, G.E. Scuseria, M.A. Robb, J.R. Cheeseman, J.A. Montgomery Jr, T. Vreven, K.N. Kudin, J.C. Burant, J.M. Millam, S.S. Iyengar, J. Tomasi, V. Barone, B. Mennucci, M. Cossi, G. Scalmani, N. Rega, G.A. Petersson, H. Nakatsuji, M. Hada, M. Ehara, K. Toyota, R. Fukuda, J. Hasegawa, M. Ishida, T. Nakajima, Y. Honda, O. Kitao, H. Nakai, M. Klene, X. Li, J.E. Knox, H.P. Hratchian, J.B. Cross, C. Adamo, J. Jaramillo, R. Gomperts, R.E. Stratmann, O. Yazyev, A.J. Austin, R. Cammi, C. Pomelli, J.W. Ochterski, P.Y. Ayala, K. Morokuma, G.A. Voth, P. Salvador, J.J. Dannenberg, V.G. Zakrzewski, S. Dapprich, A.D. Daniels, M.C. Strain, O. Farkas, D.K. Malick, A.D. Rabuck, K. Raghavachari, J.B. Foresman, J.V. Ortiz, Q. Cui, A.G. Baboul, S. Clifford, J. Cioslowski, B.B. Stefanov, G. Liu, A. Liashenko, P. Piskorz, I. Komaromi, R.L. Martin, D.J. Fox, T. Keith, M.A. Al-Laham, C.Y. Peng, A. Nanayakkara, M. Challacombe, P.M.W. Gill, B. Johnson, W. Chen, M.W. Wong, C. González, J.A. Pople, Gaussian 03, Revision C.02, GaussianInc., Wallingford, CT, 2004.
- [30] M.H. Jamróz, *Vibrational energy distribution analysis (VEDA): scopes and limitations*, *Spectrochim. Acta* 114 (2013) 220–230.
- [31] M.H. Jamróz, *Vibrational Energy Distribution Analysis VEDA4*, 2004–2010. Warsaw, <http://www.smmg.pl/>.
- [32] W. Kohn, L.J. Sham, *Phys. Rev.* 140 (1965) A1133–A1138.
- [33] J. Tomasi, b. Mennucci, R. Cammi, *Chem. Rev.* 105 (2005) 2999–3094.
- [34] L.J. Farrugia, *J. Appl. Crystallogr.* 30 (1997) 565.
- [35] S. Grabowsky, P.M. Dean, B.W. Skelton, A.N. Sobolev, M.A. Spackman, A.H. White, *CrystEngComm* 14 (2012), 1083–1083.
- [36] T.B. Richardson, S. De Gala, R.H. Crabtree, P.E.M. Siegbahn, *J. Am. Chem. Soc.* 117 (1995) 12875–12876.
- [37] A. Fu, D. Du, Z. Zhou, *Spectrochim. Acta* 59 (2003) 245–253.
- [38] A. Saeed, M.F. Erben, M. Bolte, *J. Org. Chem.* 77 (2012) 4688–4695.
- [39] N. Issaoui, H. Ghalla, F. Bardak, M. Karabacak, N. Aouled Dlala, H.T. Flakus, *J. Mol. Struct.* 1130 (2017) 659–668.
- [40] D.M. Gil, *J. Mol. Struct.* 1205 (2020) 127589.
- [41] G. Varsanyi, *Vibrational Spectra of Benzene Derivatives*, Academic Press, New York, 1969.
- [42] N. Issaoui, H. Ghalla, S.A. Brandán, F. Bardak, H.T. Flakus, A. Atac, B. Oujia, *J. Mol. Struct.* 1135 (2017) 209–221.
- [43] S. Gatfaoui, N. Issaoui, A. Mezni, F. Bardak, T. Roisnel, A. Atac, H. Marouani, *J. Mol. Struct.* 1150 (2017) 242–257.
- [44] N. Issaoui, H. Ghalla, S. Muthu, H.T. Flakus, B. Oujia, *Spectrochim. Acta* 136 (2015) 1227–1242.
- [45] M. Rocha, D.M. Gil, G.A. Echeverría, O.E. Piro, J.L. Jios, S.E. Ulic, *J. Org. Chem.* 84 (2019) 11042–11053.
- [46] J. Fleming, *Frontier Orbital's and Organic Chemical Reactions*, John Wiley & Sons, New York, 1976.
- [47] L.R. Domingo, P. Pérez, J.A. Sáez, *RSC Adv.* 3 (2013) 1486–1494.
- [48] J.P. Foster, F. Weinhold, *J. Am. Chem. Soc.* 102 (1980) 7211–7218.